ARTICLE

Multiple frequency saturation pulses reduce CEST acquisition time for quantifying conformational exchange in biomolecules

Maureen Leninger[1] · William M. Marsiglia[1] · Alexej Jerschow[1] · Nathaniel J. Traaseth[1]

Abstract

Exchange between conformational states is required for biomolecular catalysis, allostery, and folding. A variety of NMR experiments have been developed to quantify motional regimes ranging from nanoseconds to seconds. In this work, we describe an approach to speed up the acquisition of chemical exchange saturation transfer (CEST) experiments that are commonly used to probe millisecond to second conformational exchange in proteins and nucleic acids. The standard approach is to obtain CEST datasets through the acquisition of a series of 2D correlation spectra where each experiment utilizes a single saturation frequency to ^1H, ^{15}N or ^{13}C. These pseudo 3D datasets are time consuming to collect and are further lengthened by reduced signal to noise stemming from the long saturation pulse. In this article, we show how usage of a multiple frequency saturation pulse (i.e., MF-CEST) changes the nature of data collection from *series* to *parallel*, and thus decreases the total acquisition time by an integer factor corresponding to the number of frequencies in the pulse. We demonstrate the applicability of MF-CEST on a Src homology 2 (SH2) domain from phospholipase Cγ and the secondary active transport protein EmrE as model systems by collecting ^{13}C methyl and ^{15}N backbone datasets. MF-CEST can also be extended to additional sites within proteins and nucleic acids. The only notable drawback of MF-CEST as applied to backbone ^{15}N experiments occurs when a large chemical shift difference between the major and minor populations is present (typically greater than ~ 8 ppm). In these cases, ambiguity may arise between the chemical shift of the minor population and the multiple frequency saturation pulse. Nevertheless, this drawback does not occur for methyl group MF-CEST experiments or in cases where somewhat smaller chemical shift differences occur are present.

Keywords Solution NMR · CEST · Sensitivity enhancement · Fast data acquisition · Proteins

Introduction

NMR experiments over the last two decades have unveiled the importance of slow conformational motions to the discovery of molecular mechanisms underlying allostery, enzyme catalysis, and protein folding (Palmer and Massi 2006; Massi et al. 2005; Mittermaier and Kay 2009). This progress has been fostered by methodological improvements to probe biomolecular dynamics using solution NMR on a range of timescales. Faster timescales are analyzed with rotating frame and free precession relaxation dispersion experiments that under ideal conditions are able to quantify the rate of conformational exchange, the populations between the interconverting states, and the chemical shifts of higher energy conformers within the ensemble of states. Developments for probing µs to ms timescale motion include the in-phase/anti-phase CPMG relaxation dispersion experiment (Loria et al. 1999; Korzhnev et al. 2004) and the use of adiabatic pulses as the element to induce relaxation dispersion (Traaseth et al. 2012; Mangia et al. 2010). Slower motions on the ms to s timescale necessitate the usage of exchange spectroscopy (EXSY) (Gutowsky and Saika 1953; Li and Palmer 2009; Sahu et al. 2007; Montelione and Wagner 1989; Farrow et al. 1994) or chemical exchange saturation transfer (CEST) techniques (Ward et al. 2000; Vallurupalli et al. 2012; Tang

Maureen Leninger and William M. Marsiglia have contributed equally to this work.

✉ Nathaniel J. Traaseth
traaseth@nyu.edu

1 Department of Chemistry, New York University, 100 Washington Square East, New York, NY 10003, USA

et al. 2008). The former method can be employed when the populations between states are comparable, while the latter methods are useful when a minor population is in exchange with the major conformational state (Vallurupalli et al. 2012) or where the molecule is in exchange with a large molecular weight species that is unobservable by solution NMR (Fawzi et al. 2011). Biological processes occurring on this timescale include conformational changes needed for molecular transport (Gayen et al. 2016; Akyuz et al. 2013; Morrison et al. 2012), protein folding (Sekhar et al. 2015; Ma et al. 2016; Fizil et al. 2015), enzyme catalysis (Gladkova et al. 2017), and molecular recognition mechanisms (Zhao et al. 2017; Delaforge et al. 2015).

The common experimental feature of relaxation dispersion spectroscopy and CEST experiments applied to biomolecules is that the variable exchange period represents an effective third dimension (Vallurupalli et al. 2012). In other words, these datasets require a series of 2D correlation spectroscopies such as ^{1}H/^{15}N HSQC or ^{1}H/^{13}C HSQC to resolve the resonances in order to acquire site-specific information on the exchange process. Thus, the total time for these acquisitions is substantial and often requires more experimental time than a standard 3D experiment due to the signal to noise needed to derive quantitative conclusions from relaxation rates or saturation transfer stemming from chemical exchange. The best available solution for reducing the experimental duration is to employ non-linear sampling that reduces the number of indirect increments in the 2D correlation plane to resolve the signals (Long et al. 2015; Matsuki et al. 2011).

In this article, we propose an alternative method to reduce the acquisition times in CEST experiments applied to biomolecules by making use of multiple frequency saturation pulses. CEST was developed to improve contrast in magnetic resonance imaging (Ward et al. 2000; Zhou and van Zijl 2006) and the use of multiple frequency pulses has been a valuable addition for distinguishing magnetization transfer from true CEST mechanisms (Lee et al. 2012). Our experiments utilize multiple frequency saturation pulses to reduce the total time required to obtain pseudo 3D acquisitions by an integer factor corresponding to the number of frequencies incorporated within the pulse. This multiple frequency CEST method we refer to as *MF-CEST* is demonstrated with two protein systems on backbone amide ^{15}N and methyl group ^{13}C sites.

Materials and methods

Preparation of the C-terminal SH2 domain from phospholipase Cγ

The Src Homology 2 (SH2) domain from PLCγ corresponding to residues N662 to L774 was expressed in *Escherichia*

coli using a modified M9 media where the sole nitrogen source was ^{15}N ammonium chloride. In addition to ^{15}N incorporation, MILVAT methyl labeling (Proudfoot et al. 2016) was incorporated into the SH2 domain by adding the following precursors or amino acids 1 h prior to induction: L-methionine (^{13}C$^\varepsilon$) (250 mg/L); 2-ketobutyric acid-4-^{13}C,3,3-^{2}H$_2$ (50 mg/L); 2-keto-3-methyl-^{13}C-butyric-4-^{13}C,3-^{2}H acid (80 mg/L); L-alanine (3-^{13}C,2-^{2}H) (100 mg/L); L-threonine (4-^{13}C;2,3-^{2}H$_2$) (50 mg/L); glycine (^{2}H$_5$) (100 mg/L). Protein expression was induced overnight at 20 °C using 0.1 mM IPTG. The cell pellet was resuspended in 20 mM sodium phosphate buffer containing 600 μM phenylmethylsulfonyl fluoride (PMSF), 1.25 mM EDTA, 2.3 μM leupeptin, 1.45 μM pepstatin A, 5% glycerol, 8.8 μM lysozyme, and 400 μM DTT, pH 6.5, and lysed using a French press. Cell debris were removed by centrifugation, and the supernatant was concentrated using an Amicon centrifuge spin concentrator (3 kDa cutoff). Concentrated lysate was injected onto a cation exchange column (Source S, GE Healthcare, Piscataway, NJ) and eluted using a gradient of 0.025–1.0 M NaCl. Purity was assessed using SDS-PAGE. Elution from the cation exchange column was buffer exchanged into 25 mM HEPES (pH 7.5), 150 mM NaCl, 0.1% sodium azide, and 5% ^{2}H$_2$O, and concentrated to make the NMR sample consisting of 1.0 mM protein.

Preparation of EmrE sample

The expression and purification of EmrE was carried out as previously described (Gayen et al. 2013, 2016; Cho et al. 2014). EmrE was expressed as a fusion construct with maltose-binding protein and purified using affinity and size exclusion chromatography in n-dodecyl-β-D-maltopyranoside (DDM, Anatrace). [Ile-^{13}CH$_3$, Leu-^{13}CH$_3$, Val-^{13}CH$_3$ U-^{15}N, ^{2}H]-labeled EmrE was expressed with addition of 50 mg/L 2-ketobutyric acid-4-^{13}C, 3,3-^{2}H$_2$ sodium salt hydrate, and 80 mg/L of 2-keto-3-(methyl-^{2}H$_3$)-butyric acid-4-^{13}C, 3-^{2}H sodium salt 1 h prior to induction. EmrE in DDM was reconstituted into dimyristoyl-*sn*-glycero-3-phosphocholine (DMPC) and dihexanoyl-*sn*-glycero-3-phosphocholine (DHPC) bicelles at a molar ratio of 1:3. The acyl chains of DMPC and DHPC were perdeuterated (14:0 PC ^{2}H$_{54}$ and 6:0 PC ^{2}H$_{22}$; Avanti Polar Lipids) to reduce the lipid signals in ^{1}H/^{13}C heteronuclear correlation experiments. The final NMR samples contained 0.8 mM EmrE bound to tetraphenylphosphonium with a lipid to protein ratio 150:1 (DMPC:EmrE, mol:mol). The buffer was 100 mM Na$_2$HPO$_4$ (pH 5.8) and 20 mM NaCl.

MF-CEST acquisitions

All NMR datasets were acquired using a Bruker Avance III spectrometer at a ^{1}H frequency of 600 MHz equipped with

a TCI cryogenic probe. The pulse sequences used to incorporate multiple frequency saturation pulses were the same as those described by Kay and co-workers (Vallurupalli et al. 2012; Bouvignies and Kay 2012). Shaped pulses were generated with one-, two-, or three-frequencies with a pulse length of 0.4 s (cSH2) or 0.5 s (EmrE) using a total of 40,000 points. The Bruker python script used to create the multiple frequency pulses is available for download at https://github.com/jaeseung16/NMR_Bruker/blob/master/python/multifreq.py. During the saturation period, ^{1}H decoupling was applied as a composite block of $90_x240_y90_x$ (Vallurupalli et al. 2012; Levitt 1982) at rf field strengths ($\omega_1/2\pi$) of 3.1 and 5 kHz for ^{15}N and ^{13}C experiments, respectively. Note that the presence of small decoupling dips has been reported as a result of ^{1}H composite pulse decoupling (Vallurupalli et al. 2012). Although we did not observe these dips in our experiments, it is possible these artifacts will appear in very concentrated samples, which will be positioned $\pm 1/(2pw)$ from the primary resonance, where pw is $1.17/(^1$H rf field) as reported by Vallurupalli et al. (Vallurupalli et al. 2012). If these decoupling dips are observed, one can increase the decoupling field strength to avoid interference with a true exchange dip or ignore them in subsequent data analysis.

One-frequency CEST experiments on ^{15}N labeled cSH2 were acquired using a total of 59×2D acquisitions (1 reference and 58 CEST experiments) with saturation frequencies ranging from 103.5 to 132 ppm in steps of 0.5 ppm at an applied rf field strength of 25 Hz. Two-frequency MF-CEST experiments were acquired using 29×2D experiments (1 reference and 28 MF-CEST experiments) with saturation frequencies ranging from 104 to 131.5 ppm. Due to the two-frequency nature of the saturation pulse, the first experiment utilized saturation frequencies of 104 and 118 ppm. In each subsequent experiment, the saturation offset was increased by 0.5 ppm for both frequencies. The three-frequency MF-CEST experiments were collected using 20×2D experiments (1 reference and 19 MF-CEST experiments) with saturation frequencies ranging from 103.5 to 131.5 ppm. The three-frequency experiments utilized offsets of 103.5, 113, and 122.5 ppm in the first experiment. In each subsequent experiment the offsets were shifted by 0.5 ppm. The spectral widths and sampling times were 1703 Hz and 23.5 ms for ^{15}N and 10,000 Hz and 82.9 ms for ^{1}H, respectively. The recycle delay was 1.5 s.

Methyl MF-CEST experiments applied to MILVAT labeled cSH2 were acquired in a similar fashion as the backbone ^{15}N experiments at a temperature of 25 °C. One-frequency CEST was acquired using 100×2D experiments (1 reference, 99 CEST) with the ^{13}C saturation frequency ranging from 7.24 to 31.74 ppm in steps of 0.25 ppm. Three-frequency MF-CEST consisted of 34×2D experiments (1 reference, 33 MF-CEST) where the ^{13}C saturation frequencies were spaced by 8.25 ppm. The initial experiment employed saturation frequencies at 7.24, 15.49, and 23.74 ppm. Subsequent 2D experiments were frequency shifted by 0.25 ppm. The field strength for the one-frequency saturation pulse was 15 Hz ($\omega_1/2\pi$). The three-frequency MF-CEST pulse was increased in power by 9.54 dB. The spectral widths and sampling times were 3773 Hz and 13.3 ms for ^{13}C and 10,000 Hz and 59.9 ms for ^{1}H, respectively. The recycle delay was 1.5 s and each experiment was collected with 4 scans at a temperature of 25 °C.

Methyl one-frequency CEST and two-frequency MF-CEST experiments were acquired on EmrE at a temperature of 37 °C. The one-frequency experiment was acquired with 24×2D experiments (1 reference, 23 CEST) with saturation frequencies ranging from 9.6 to 16.2 ppm in steps of 0.3 ppm. Two-frequency MF-CEST was acquired with the same number of experiments, but also utilized a second frequency excitation shifted by 10 ppm (i.e., start at 19.6 ppm). The spectral widths and sampling times were 4000 Hz and 9.75 ms for ^{13}C and 10,000 Hz and 59.9 ms ^{1}H, respectively. The recycle delay was 1.5 s and each experiment was acquired with 32 scans. The experiment was repeated in duplicate and the average of these datasets is displayed. All pseudo 3D acquisitions on cSH2 or EmrE were acquired in an interleaved fashion.

Determination of exchange rate from CEST curves

CEST curves were fit using *chemex* (https://github.com/gbouvignies/chemex) in a similar manner as previously described (Vallurupalli et al. 2012). Namely, the relaxation rate R_1 was fixed to be the same for the two populations in exchange and we modeled the B_1 homogeneity in a similar manner, although changes to the homogeneity did not influence the fitted parameters. Due to the unique features of the EmrE asymmetric dimer (Gayen et al. 2016; Cho et al. 2014; Morrison et al. 2012), the populations of the two states were each fixed to 0.5 and the ^{13}C chemical shifts of the two exchanging species were also fixed to their values measured directly from the ^{1}H/^{13}C HSQC spectrum (Gayen et al. 2016; Cho et al. 2014). We also chose to fix the relaxation rate R_2 to the same value for two exchanging populations, because the linewidths for the two populations were quite similar. Global and individual fits to the exchange rate (k_{ex}) were carried out for CEST and MF-CEST curves acquired on EmrE. A total of six curves were fit for CEST or MF-CEST profiles that corresponded to three residues (I54, I58, and I68). The global fits yielded a single value for each dataset, while individual fits yielded six values for the six sites. The average and standard deviation among individual fitted residues were also calculated and reported in the main text.

Results and discussion

Multiple frequency CEST (MF-CEST)

CEST experiments on proteins and nucleic acids are collected through the acquisition of a series of HSQC-type spectra where each 2D experiment employs a single saturation frequency to longitudinal magnetization (Vallurupalli et al. 2012; Bouvignies and Kay 2012). For ^{15}N labeled proteins at the backbone, this involves sweeping over ~ 30 ppm in steps of 0.25–0.5 ppm, which requires 60–120 × 2D correlation experiments. In addition to the pseudo 3D nature of the experiment, the relatively long saturation pulse needed to observe conformational exchange further lowers the signal to noise and increases the experimental acquisition time. With the goal of decreasing the total time required for CEST data collection, we envisioned an approach that uses saturation pulses consisting of multiple frequencies to enable data acquisition *in parallel* rather than the standard manner *in series*. We will refer to this method as multiple frequency CEST or *MF-CEST* (see scheme in Fig. 1a). It should be noted that the major limitation to MF-CEST is that application of multiple frequency pulses can concurrently saturate both the major and minor populations, which would mask the observed conformational exchange. This will occur if the chemical shift difference between the exchanging sites were coincident with the difference in frequencies
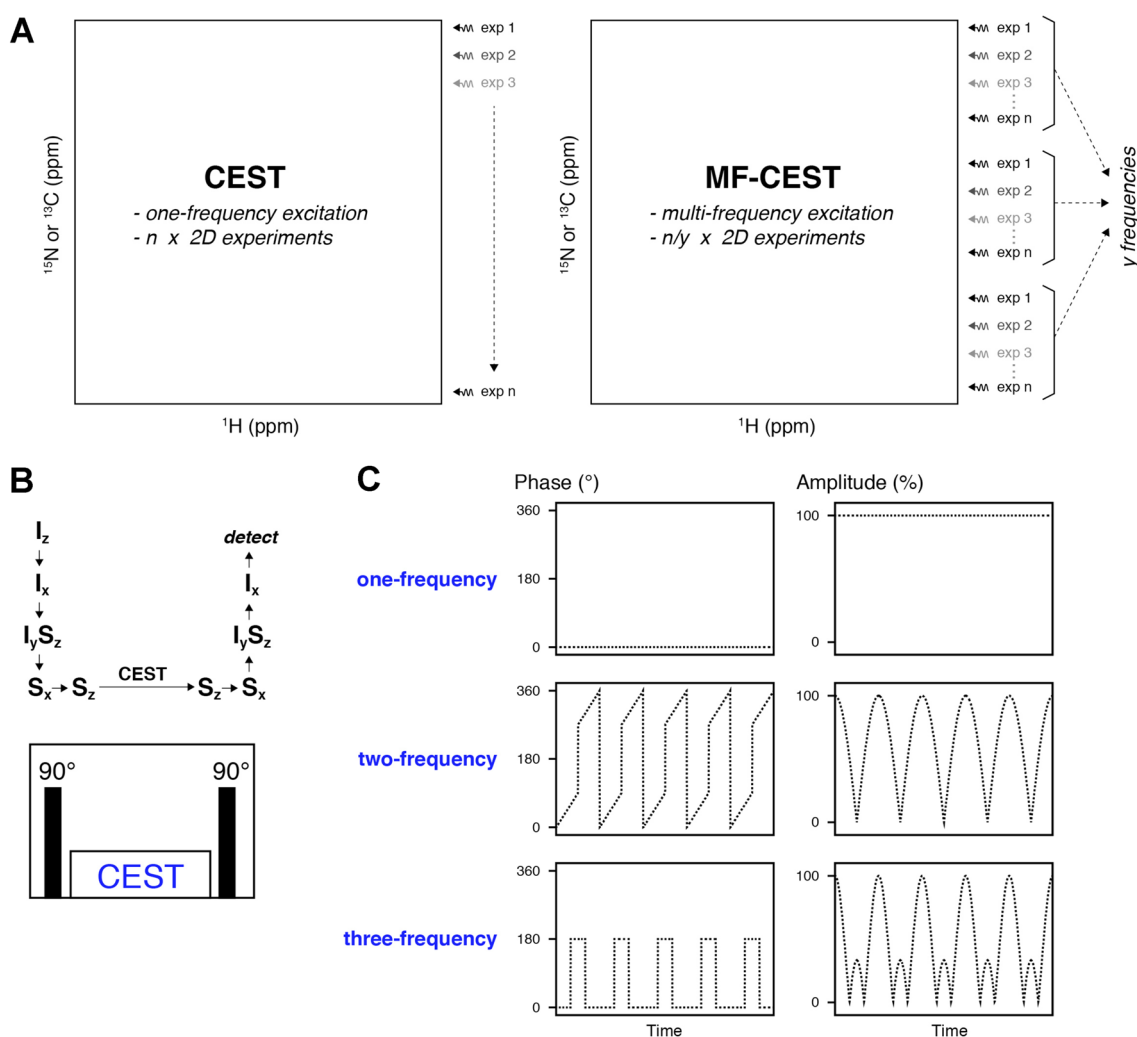

Fig. 1 **a** Schematic of CEST and MF-CEST. Standard CEST acquisitions exhaustively sample all offset frequencies (i.e., *in series*), while the MF-CEST approach applies n frequencies at the same time and therefore can reduce the number of 2D acquisitions necessary (i.e., *in parallel*). **b** Magnetization flow for implementation of heteronuclear CEST experiments with saturation pulses on *X* nuclei (e.g., ^{15}N or ^{13}C). The CEST period in the pulse sequence schematic is shown for the *X* nuclei only. **c** Schematic of amplitude and phase modulation applied during the CEST period within (**b**)

Table 1 Saturation frequencies for ^{15}N MF-CEST experiments on cSH2

Experiment	Two-frequency (ppm)		Three-frequency (ppm)		
1	104.0	118.0	103.5	113.0	122.5
2	104.5	118.5	104.0	113.5	123.0
3	105.0	119.0	104.5	114.0	123.5
4	105.5	119.5	105.0	114.5	124.0
5	106.0	120.0	105.5	115.0	124.5
6	106.5	120.5	106.0	115.5	125.0
7	107.0	121.0	106.5	116.0	125.5
8	107.5	121.5	107.0	116.5	126.0
9	108.0	122.0	107.5	117.0	126.5
10	108.5	122.5	108.0	117.5	127.0
11	109.0	123.0	108.5	118.0	127.5
12	109.5	123.5	109.0	118.5	128.0
13	110.0	124.0	109.5	119.0	128.5
14	110.5	124.5	110.0	119.5	129.0
15	111.0	125.0	110.5	120.0	129.5
16	111.5	125.5	111.0	120.5	130.0
17	112.0	126.0	111.5	121.0	130.5
18	112.5	126.5	112.0	121.5	131.0
19	113.0	127.0	112.5	122.0	131.5
20	113.5	127.5			
21	114.0	128.0			
22	114.5	128.5			
23	115.0	129.0			
24	115.5	129.5			
25	116.0	130.0			
26	116.5	130.5			
27	117.0	131.0			
28	117.5	131.5			

used for MF-CEST. In our applications detailed below, the difference in frequencies for MF-CEST is ~ 10 ppm or more, and therefore would lead to masking when the two populations have relatively large chemical shift differences. To the contrary, if the chemical shift differences are less than ~ 5–7 ppm (i.e., the typical case), then MF-CEST will have no ambiguity and allow for substantial reductions in data collection times. A second limitation related to the ambiguity created by the multiple frequency saturation pulse may occur if the minor site has a broad-band spectral signature, such as when an aggregate is studied (Fawzi et al. 2011; Milojevic et al. 2007) or in the presence of paramagnetic interactions (Hansen and Led 2006). Under these circumstances the MF-CEST experiment may not provide a sufficiently unambiguous assignment of the exchanging sites.

To implement MF-CEST, we designed shaped pulses incorporating one, two, or three frequencies with equally spaced offsets by combining the appropriately modulated components (see schematic example in Fig. 1b). As an example of two-frequency MF-CEST applied to ^{15}N, we set the two CEST frequencies in the first 2D experiment to 104 and 118 ppm. The next experiment shifted the excitation frequencies by 0.5 ppm to produce the two-frequency saturations at 104.5 and 118.5 ppm. In each subsequent experiment, the frequencies were shifted by 0.5 ppm until the final frequency set of 117.5 and 131.5 ppm. All offsets used in the MF-CEST experiments are shown in Table 1. The second difference from the standard CEST experiment is that the overall power with which the shaped saturation pulse is executed requires adjustment for the number of frequency components. Specifically, the number of applied frequencies (n) increases the power in dB proportional to $20 \log n$ relative to a single frequency saturation. Hence, a two-frequency saturation requires 6.02 dB greater power, while a three-frequency pulse requires 9.45 dB more power relative to one-frequency CEST. In other words, the power in watts will be fourfold higher for two frequencies and ninefold higher for three frequencies (i.e., power scales with n^2). As a result, each individual saturation component would be executed at
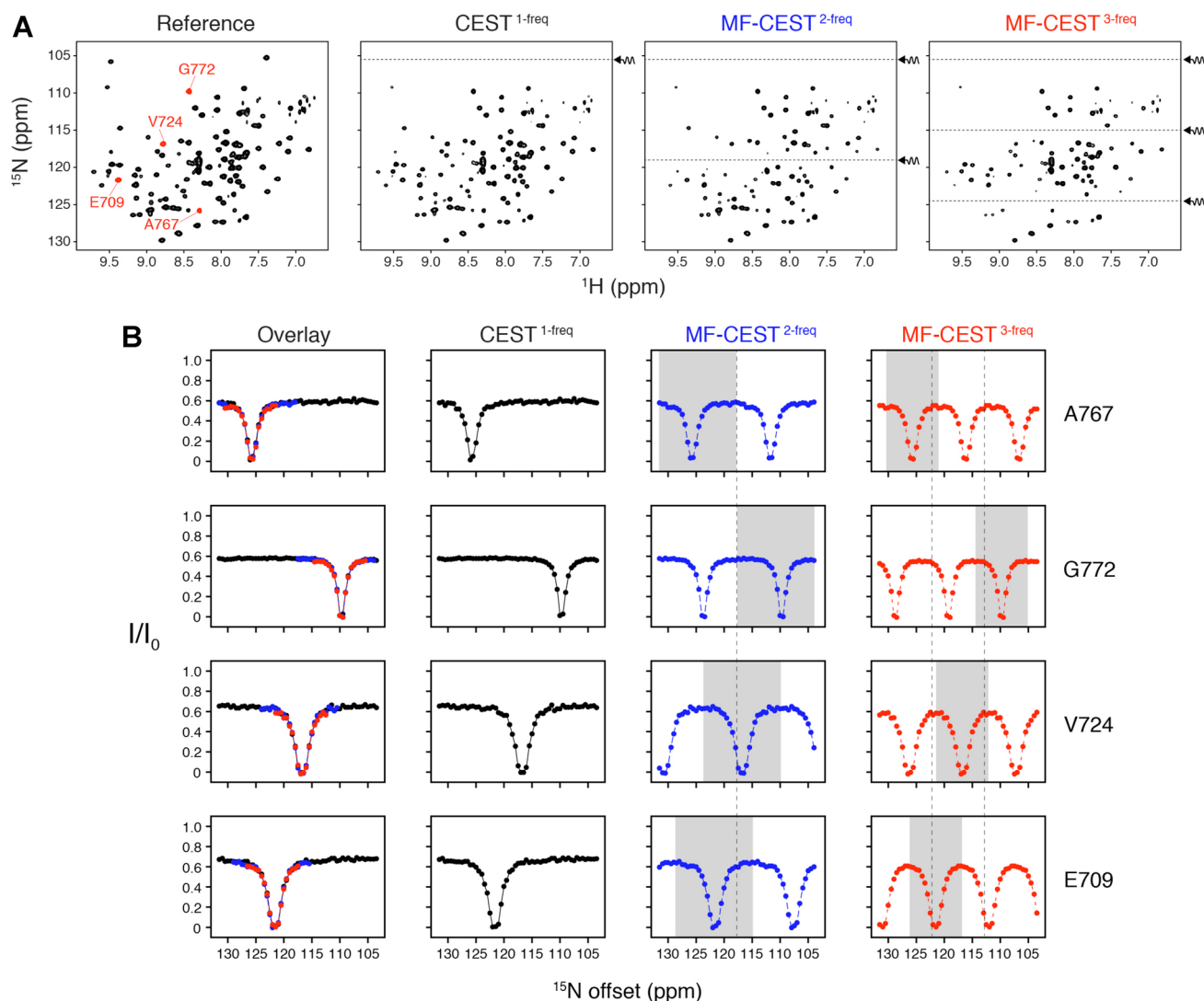
Fig. 2 ^{15}N CEST experiments applied to the cSH2 domain of PLCγ. **a** Example 2D spectra of the reference dataset, one-frequency CEST, and two- and three-frequency MF-CEST. The latter two spectra emphasize that two and three dips are created within the spectra (dotted lines indicate the application of rf saturation pulses). **b** CEST profiles for select residues highlighted in the reference spectrum shown in (**a**). The overlay displayed on the left column illustrates the region of the MF-CEST curve that can be interpreted in an unambiguous manner to exchange (also highlighted in grey in individual MF-CEST profiles). The width of the saturation dip can be reduced by employing a reduced rf field (i.e., less than 25 Hz), which would enable better resolution of exchanging populations. However, no residues in cSH2 showed the presence of conformational exchange. Note that for the MF-CEST^{2-freq} and MF-CEST^{3-freq} columns in (**b**), the white and grey regions are identical data points, which stems from the ambiguity of the multiple frequency excitations

the same nominal nutation frequency as a single-frequency saturation pulse. The increased power is not a limitation for two- or three-frequency MF-CEST since the rf field strength ($\omega_1/2\pi$) is proportional to the peak linewidth and thus typical nutation frequencies range from 10 to 40 Hz. This relatively small field strength means that the increased power for MF-CEST is not a limiting factor on the probe or spectrometer hardware and does not lead to any adverse effects.

We incorporated our MF-CEST pulses into the ^{1}H/^{15}N HSQC-CEST pulse sequence as previously described (Vallurupalli et al. 2012) and applied this to the C-terminal

SH2 domain (cSH2) from phospholipase Cγ (PLCγ). This enzyme is activated upon recruitment and subsequent phosphorylation by receptor tyrosine kinases and was recently shown to be involved in a 1:2 complex between PLCγ and the fibroblast growth factor receptor (Huang et al. 2016). The cSH2 protein was labeled with ^{15}N and ^{13}C at methyl group residues corresponding to Ile, Leu, Val, Met, Thr, and Ala. For ^{15}N CEST experiments, we acquired the traditional one-frequency CEST experiment as well as two- and three-frequency MF-CEST experiments through the application of a 0.4 s saturation pulse in the presence of ^{1}H decoupling

as previously described (Vallurupalli et al. 2012; Bouvignies and Kay 2012). A reference spectrum with no saturation delay was also acquired in order to calculate reference peak intensities (I_0). The total acquisition times for the one-, two-, and three-frequency experiments were 20, 10, and 7 h, respectively. Example 2D spectra from the reference, one-frequency CEST, and two- and three-frequency MF-CEST are shown in Fig. 2a. As observed in these spectra, the primary difference from the standard one-frequency CEST experiment is that the MF-CEST datasets have two or three horizontal holes in the spectra as indicated by dotted lines. CEST profiles (I/I_0 vs. offset) from our pseudo 3D experiments are shown for several residues within the cSH2 domain in Fig. 2b. In one-frequency CEST curves, we did not observe additional dips in the CEST profiles at 25 °C that would support the presence of slow chemical exchange between two or more conformations, and therefore this sample served as a control for comparing the standard CEST acquisition with MF-CEST. The overlay of CEST and MF-CEST results shows that our approach reproduces the shape of the standard one-frequency experiment and therefore can be used to reduce the time for acquisition by two to three-fold depending on whether two- or three-frequency MF-CEST is carried out. It is important to note that the rf field strength for saturation was set to be relatively high ($\omega_1/2\pi = 25$ Hz) in the experiments shown in Fig. 2, which led to relatively broad CEST dips. For exchange processes involving small chemical shift differences, this saturation field should be reduced, which would narrow the width of the dip and enable better resolution of lowly populated exchange populations. Finally, we note that Gly residues are often located in a specific frequency location in the ^{15}N spectrum, and therefore a minimalist use of ^{15}N MF-CEST would be to employ a two-frequency shaped pulse where one frequency scans from ~ 100 to 115 ppm and a second that ranges from ~ 115 to 130 ppm. This would further reduce possible masking of lowly populated states undergoing slow conformational exchange with the major state and the ambiguity of the resulting dataset.

MF-CEST applied to ^{13}C methyl groups

Methyl group labeling of proteins with $-^{13}CH_3$ in a per-deuterated background has substantial benefits that include increased sensitivity, resolution, and the ability to study macromolecular systems not accessible with detection of the polypeptide backbone (Tugarinov and Kay 2005). Initial labeling procedures focused on Ile, Leu, and Val (*ILV*) (Rosen et al. 1996) and recent efforts have further extended labeling to all methyl sites in proteins (*MILVAT*) (Proudfoot et al. 2016). The broad usage of this labeling strategy in the protein NMR field motivated us to investigate the use of MF-CEST to methyl labeled proteins. ^{13}C chemical shifts

of methyl groups span ~ 25 ppm and due to the narrower linewidths of these experiments, the required step size for CEST experiments is ~ 0.25 ppm or less. This requires at least $100 \times 2D$ HSQC-type experiments in order to saturate each possible methyl chemical shift frequency. A major benefit of MF-CEST applied to methyl groups is that ^{13}C chemical shifts cluster in specific regions, which is emphasized in the plot in Fig. 3a where the values were obtained from the BMRB database on diamagnetic proteins (Ulrich et al. 2008). As can be surmised from this plot, it is uncommon to observe ^{13}C methyl chemical shift changes by more than ~ 5 ppm. Therefore, the benefit for using ^{13}C MF-CEST to probe slow conformational exchange in methyl labeled samples is even greater than the ^{15}N based MF-CEST experiments (i.e., the masking effect is essentially negligible).

To carry out ^{13}C CEST experiments, we used the ^{1}H/^{13}C HSQC-CEST pulse sequence described by Bouvignies and Kay (2012) and acquired a standard one-frequency CEST dataset along with a three-frequency MF-CEST experiment on MILVAT labeled cSH2 domain (reference 2D correlation spectrum shown in Fig. 3b). The one-frequency CEST dataset consisted of $100 \times 2D$ experiments (1 reference, 99 CEST) where the ^{13}C saturation frequency was changed from 7.24 to 31.74 ppm in steps of 0.25 ppm. The three-frequency CEST consisted of $34 \times 2D$ experiments (1 reference, 33 CEST) where the ^{13}C saturation frequencies were spaced by 8.25 ppm. The first MF-CEST experiment used a pulse consisting of saturation frequencies at 7.24, 15.49, and 23.74 ppm. Subsequent 2D experiments employed a frequency shift by 0.25 ppm in the same way as the one-frequency CEST dataset (all frequencies are listed in Table 2). A comparison of CEST profiles is shown in Fig. 3c. Similar to ^{15}N experimental results, the CEST I/I_0 intensities as a function of offset overlay closely with those from MF-CEST, which validates the use of MF-CEST experiments to reduce the total acquisition time by a factor of threefold when using a three-frequency saturation pulse.

Note that MF-CEST can also be carried out with $-CHD_2$ labeling as has recently been shown to give sensitivity enhancement factors of two- to five-fold over the standard $-CH_3$ labeling experiments (Rennella et al. 2015). Additional speedup for methyl groups is conceivable by implementing ultrafast CEST methodology whereby the saturation frequencies would be spatially encoded (Xu et al. 2013; Boutin et al. 2013). The use of this approach would likely come at a sensitivity cost, and may not be universally applicable, although advantages from one-shot operation could be exploited especially when polarization would vary, such as in hyperpolarization experiments, or when real-time conformational changes are tracked.
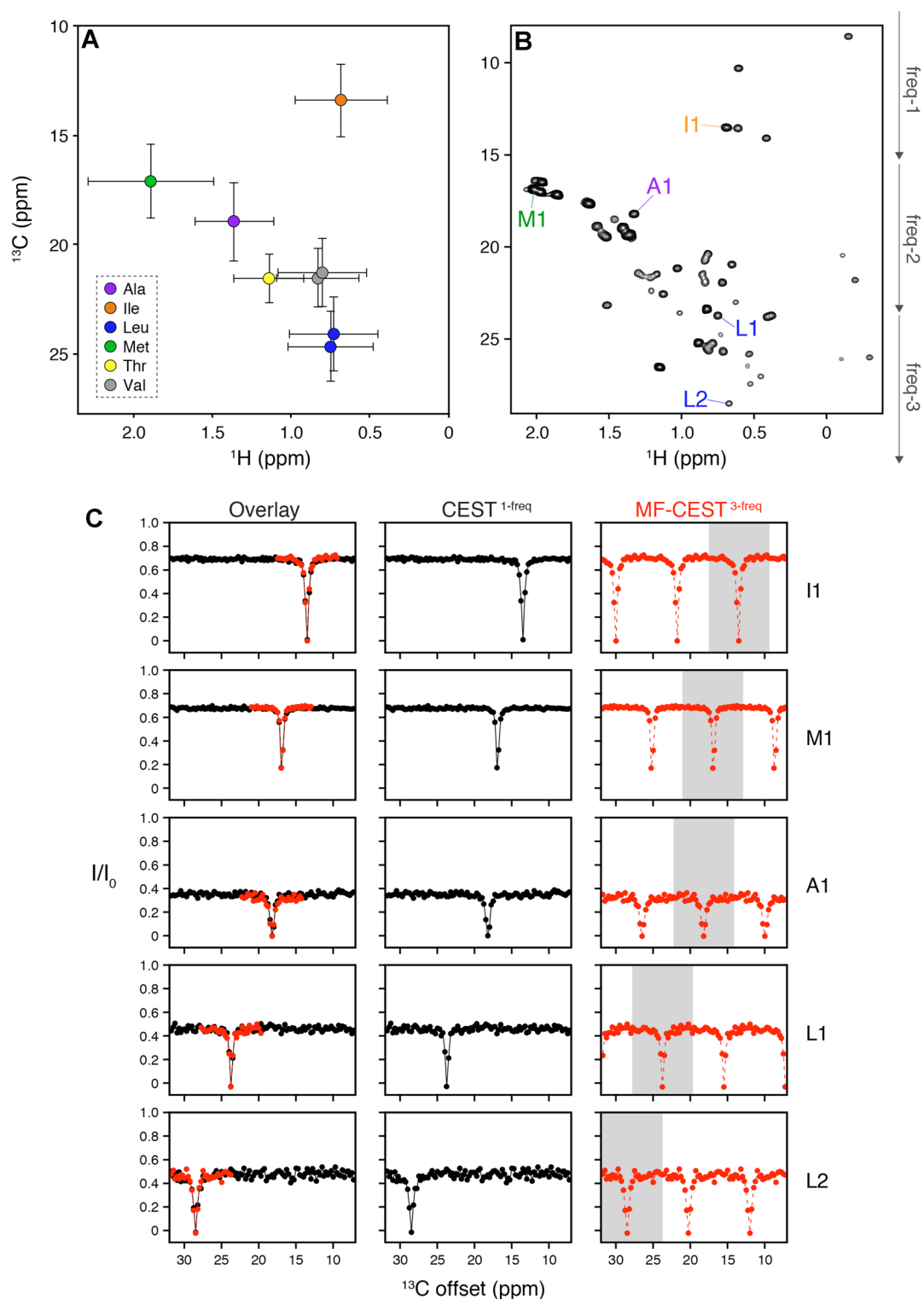
Fig. 3 Application of MF-CEST to ^{13}C MILVAT labeled cSH2. **a** Average and standard deviation for methyl group chemical shifts from diamagnetic proteins as obtained from the BMRB database (Ulrich et al. 2008). **b** HMQC spectrum shown for MILVAT labeled cSH2. **c** CEST profiles for select unassigned residues highlighted in the spectrum shown in (**b**). The overlay shows the part of the MF-CEST curve that is interpretable to exchanging populations on a slow timescale (also highlighted in grey in individual MF-CEST profiles). Note that for the MF-CEST^{3-freq} column in (**c**), the white and grey regions correspond to identical data points, which stems from the ambiguity of the multiple frequency excitations. Nevertheless, due to the frequency separation of specific methyl ^{13}C chemical shifts shown in panel (**a**), it is unlikely that methyl-based MF-CEST experiments will lead to ambiguous data interpretation

Table 2 Saturation frequencies for ^{13}C MF-CEST experiments on cSH2

Experiment	Three-frequency (ppm)		
1	7.24	15.49	23.74
2	7.49	15.74	23.99
3	7.74	15.99	24.24
4	7.99	16.24	24.49
5	8.24	16.49	24.74
6	8.49	16.74	24.99
7	8.74	16.99	25.24
8	8.99	17.24	25.49
9	9.24	17.49	25.74
10	9.49	17.74	25.99
11	9.74	17.99	26.24
12	9.99	18.24	26.49
13	10.24	18.49	26.74
14	10.49	18.74	26.99
15	10.74	18.99	27.24
16	10.99	19.24	27.49
17	11.24	19.49	27.74
18	11.49	19.74	27.99
19	11.74	19.99	28.24
20	11.99	20.24	28.49
21	12.24	20.49	28.74
22	12.49	20.74	28.99
23	12.74	20.99	29.24
24	12.99	21.24	29.49
25	13.24	21.49	29.74
26	13.49	21.74	29.99
27	13.74	21.99	30.24
28	13.99	22.24	30.49
29	14.24	22.49	30.74
30	14.49	22.74	30.99
31	14.74	22.99	31.24
32	14.99	23.24	31.49
33	15.24	23.49	31.74

Application of MF-CEST to a membrane protein with millisecond timescale dynamics

MF-CEST applied to the cSH2 domain from PLCγ demonstrated the feasibility of our method for reducing the total acquisition time for CEST acquisitions. To demonstrate this approach can also be used in cases of conformational exchange, we used the multidrug transporter EmrE bound to tetraphenylphosphonium that has previously been shown to undergo slow conformational exchange (Cho et al. 2014; Morrison et al. 2012). EmrE forms an anti-parallel and asymmetric dimer (Chen et al. 2007; Tate et al. 2003; Ubarretxena-Belandia et al. 2003) important for bacterial detoxification (Schuldiner 2009) such that each monomer within

the dimer gives rise to separate chemical shift frequencies. It has been established that the two populations for each residue within EmrE exchange in both the drug-free and drug-bound forms (Gayen et al. 2016; Cho et al. 2014; Morrison et al. 2012). Recently, we demonstrated that the conformational exchange rate can be modulated by the presence of a substrate, either proton or drug (Gayen et al. 2016; Cho et al. 2014; Banigan et al. 2018). To carry out MF-CEST, we labeled EmrE at ^{13}C methyl sites using the ILV labeling strategy in a perdeuterated background (see 2D ^{1}H/^{13}C spectrum in Fig. 4a). Previously, we published the chemical shift assignment of Ile residues and therefore focused on these sites (Gayen et al. 2016). While the use of CEST is not required to quantify conformational exchange in EmrE since it consists of a 50/50 population split between the two monomers, it provides a control for CEST experiments since the exchange has been validated using EXSY (Gayen et al. 2016; Morrison et al. 2012). We acquired one-frequency CEST and two-frequency MF-CEST over the Ile region of the spectrum. The second frequency in MF-CEST was applied over the Leu/Val region of the ^{13}C spectrum. Similar to the experimental results obtained for the cSH2 domain of PLCγ, we observed that CEST profiles were superimposable between one-frequency CEST and two-frequency MF-CEST. However, in the case of EmrE, we observed two dips in I/I_0 versus offset profiles for several residues, which stemmed from exchange between the asymmetric monomers within the dimer. Specifically, Fig. 4b shows CEST curves for residues that have different chemical shifts for the two populations (see I54, I58, and I68). As expected, the populations for the two I68 methyl resonances each show the dip that matches the frequency of the other in the respective CEST curves (see dotted lines in Fig. 4). Residues where the ^{13}C chemical shifts for the two populations are the same (I5) or very similar (I88) do not show two discrete dips in their respective CEST profiles. In order to determine the exchange rate for EmrE using these datasets, we carried out global fits of CEST curves for residues displaying two distinguishable dips (i.e., I54, I58, I68) for the CEST and MF-CEST experiments and obtained k_{ex} values of 2.4 ± 0.2 and 2.1 ± 0.2 s^{-1}, respectively. Globally fitted curves are shown in the supporting information. We also carried out individual fits to residues in CEST and MF-CEST, and these yielded average k_{ex} values of 2.7 ± 0.9 s^{-1} and 2.3 ± 0.5, respectively, where the error is the standard deviation among the six fitted residues. These fitted values suggest CEST and MF-CEST yield indistinguishable exchange rates given the error in the measurements, and therefore validate the use of MF-CEST to probe systems that undergo slow conformational exchange.
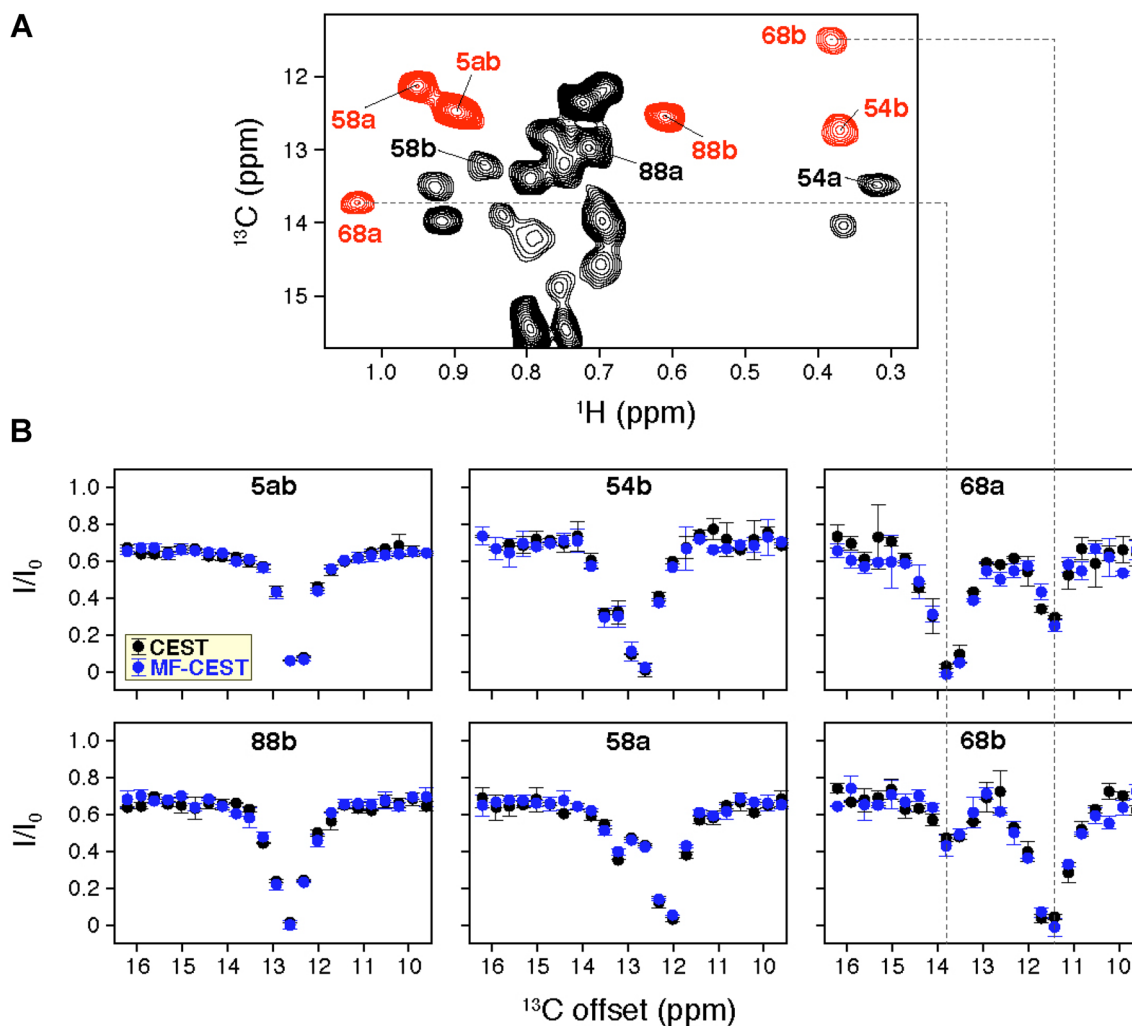
Fig. 4 CEST and MF-CEST applied to a system with conformational exchange. **a** Reference HMQC spectrum for ILV labeled EmrE in a perdeuterated background and bound to tetraphenylphosphonium. **b** Overlay of CEST (black) and MF-CEST (blue) curves for the Ile region of the spectrum. I5 and I88 show minimal chemical shift dif- ferences in the ^{13}C dimension, while I54, I58, and I68 show the pres- ence of two CEST dips that support the presence of exchange. The CEST dips for 68a and 68b match the respective curves (see dotted lines), which further emphasizes the ability to use MF-CEST for reducing the time needed for data collection

Conclusion

In this work, multiple frequency saturation pulses for CEST acquisitions were implemented and are referred to as *MF-CEST*. Since the standard way to collect CEST datasets utilizes a series of 2D experiments that each employ a sin- gle saturation frequency, the use of MF-CEST can reduce the total experimental time by a factor of two or three- fold depending on the number of saturation frequencies incorporated into the pulse. Alternatively, one can employ MF-CEST by maintaining the same overall experimen- tal acquisition time and increase the number of points in the profile by two to three-fold, which would enable one to more clearly identify the exchange dip. A limitation of MF-CEST arises when the frequency difference between the

multiple saturation pulses is similar to the frequency differ- ence between peaks undergoing conformational exchange. In this circumstance, MF-CEST can potentially mask the minor population dip within the CEST profile. This would occur for relatively large chemical shift differences between the states in exchange (i.e., greater than ~ 8 ppm). Neverthe- less, for systems with smaller chemical shift differences, this problem does not appear. In fact, application of this method to methyl groups in macromolecules offers one of the great- est advantages due to the relatively large ^{13}C spectral range and narrow linewidths for these sites. Use of MF-CEST in these cases is unlikely to lead to ambiguity due to the fact that methyl-containing residues tend to cluster into specific frequency ranges. Finally, MF-CEST can be extended to other sites within proteins and nucleic acids, such as C^α or

C^β for protein based experiments, which have excellent frequency separation yet cover a large range of ^{13}C chemical shifts.

References

Akyuz N, Altman RB, Blanchard SC, Boudker O (2013) Transport dynamics in a glutamate transporter homologue. Nature 502:114

Banigan JR, Leninger M, Her AS, Traaseth NJ (2018) Assessing interactions between a polytopic membrane protein and lipid bilayers using differential scanning calorimetry and solid-state NMR. J Phys Chem B 122:2314–2322

Boutin C, Leonce E, Brotin T, Jerschow A, Berthault P (2013) Ultrafast Z-spectroscopy for (129)Xe NMR-based sensors. J Phys Chem Lett 4:4172–4176

Bouvignies G, Kay LE (2012) A 2D (1)(3)C-CEST experiment for studying slowly exchanging protein systems using methyl probes: an application to protein folding. J Biomol NMR 53:303–310

Chen YJ et al (2007) X-ray structure of EmrE supports dual topology model. Proc Natl Acad Sci USA 104:18999–19004

Cho MK, Gayen A, Banigan JR, Leninger M, Traaseth NJ (2014) Intrinsic conformational plasticity of native EmrE provides a pathway for multidrug resistance. J Am Chem Soc 136:8072–8080

Delaforge E et al (2015) Large-scale conformational dynamics control H5N1 influenza polymerase PB2 binding to import in alpha. J Am Chem Soc 137:15122–15134

Farrow NA, Zhang O, Forman-Kay JD, Kay LE (1994) A heteronuclear correlation experiment for simultaneous determination of 15N longitudinal decay and chemical exchange rates of systems in slow equilibrium. J Biomol NMR 4:727–734

Fawzi NL, Ying J, Ghirlando R, Torchia DA, Clore GM (2011) Atomic-resolution dynamics on the surface of amyloid-beta protofibrils probed by solution NMR. Nature 480:268–272

Fizil A, Gaspari Z, Barna T, Marx F, Batta G (2015) "Invisible" conformers of an antifungal disulfide protein revealed by constrained cold and heat unfolding, CEST-NMR experiments, and molecular dynamics calculations. Chemistry 21:5136–5144

Gayen A, Banigan JR, Traaseth NJ (2013) Ligand-induced conformational changes of the multidrug resistance transporter EmrE probed by oriented solid-state NMR spectroscopy. Angew Chem Int Ed Engl 52:10321–10324

Gayen A, Leninger M, Traaseth NJ (2016) Protonation of a glutamate residue modulates the dynamics of the drug transporter EmrE. Nat Chem Biol 12:141–145

Gladkova C et al (2017) An invisible ubiquitin conformation is required for efficient phosphorylation by PINK1. EMBO J 36:3555–3572

Gutowsky HS, Saika A (1953) Dissociation, chemical exchange, and the proton magnetic resonance in some aqueous electrolytes. J Chem Phys 21:1688–1694

Hansen DF, Led JJ (2006) Determination of the geometric structure of the metal site in a blue copper protein by paramagnetic NMR. Proc Natl Acad Sci USA 103:1738–1743

Huang Z et al (2016) Two FGF receptor kinase molecules act in concert to recruit and transphosphorylate phospholipase Cgamma. Mol Cell 61:98–110

Korzhnev DM, Kloiber K, Kanelis V, Tugarinov V, Kay LE (2004) Probing slow dynamics in high molecular weight proteins by methyl-TROSY NMR spectroscopy: application to a 723-residue enzyme. J Am Chem Soc 126:3964–3973

Lee JS, Regatte RR, Jerschow A (2012) Isolating chemical exchange saturation transfer contrast from magnetization transfer asymmetry under two-frequency rf irradiation. J Magn Reson 215:56–63

Levitt MH (1982) Symmetrical composite pulse sequences for NMR population-inversion. 2. Compensation of resonance offset. J Magn Reson 50:95–110

Li Y, Palmer AG III (2009) TROSY-selected ZZ-exchange experiment for characterizing slow chemical exchange in large proteins. J Biomol NMR 45:357–60

Long D, Delaglio F, Sekhar A, Kay LE (2015) Probing invisible, excited protein states by non-uniformly sampled pseudo-4D CEST spectroscopy. Angew Chem Int Ed 54:10507–10511

Loria JP, Rance M, Palmer AG III (1999) A relaxation-compensated Carr–Purcell–Meiboom–Gill sequence for characterizing chemical exchange by NMR spectroscopy. J Am Chem Soc 121:2331–2332

Ma RS et al (2016) Determination of pseudocontact shifts of low-populated excited states by NMR chemical exchange saturation transfer. Phys Chem Chem Phys 18:13794–13798

Mangia S, Traaseth NJ, Veglia G, Garwood M, Michaeli S (2010) Probing slow protein dynamics by adiabatic R(1rho) and R(2rho) NMR experiments. J Am Chem Soc 132:9979–9981

Massi F, Grey MJ, Palmer AG III (2005) Microsecond timescale backbone conformational dynamics in ubiquitin studied with NMR R1rho relaxation experiments. Prot Sci 14:735–742

Matsuki Y, Konuma T, Fujiwara T, Sugase K (2011) Boosting protein dynamics studies using quantitative nonuniform sampling NMR spectroscopy. J Phys Chem B 115:13740–13745

Milojevic J, Esposito V, Das R, Melacini G (2007) Understanding the molecular basis for the inhibition of the Alzheimer's Abeta-peptide oligomerization by human serum albumin using saturation transfer difference and off-resonance relaxation NMR spectroscopy. J Am Chem Soc 129:4282–4290

Mittermaier AK, Kay LE (2009) Observing biological dynamics at atomic resolution using NMR. Trends Biochem Sci 34:601–611

Montelione GT, Wagner G (1989) 2d chemical-exchange NMR-spectroscopy by proton-detected heteronuclear correlation. J Am Chem Soc 111:3096–3098

Morrison EA et al (2012) Antiparallel EmrE exports drugs by exchanging between asymmetric structures. Nature 481:45–50

Palmer AG III, Massi F (2006) Characterization of the dynamics of biomacromolecules using rotating-frame spin relaxation NMR spectroscopy. Chem Rev 106:1700–1719

Proudfoot A, Frank AO, Ruggiu F, Mamo M, Lingel A (2016) Facilitating unambiguous NMR assignments and enabling higher probe density through selective labeling of all methyl containing amino acids. J Biomol NMR 65:15–27

Rennella E, Huang R, Velyvis A, Kay LE (2015) (13)CHD2-CEST NMR spectroscopy provides an avenue for studies of conformational exchange in high molecular weight proteins. J Biomol NMR 63:187–199

Rosen MK et al (1996) Selective methyl group protonation of perdeuterated proteins. J Mol Biol 263:627–636

Sahu D, Clore GM, Iwahara J (2007) TROSY-based z-exchange spectroscopy: application to the determination of the activation energy for intermolecular protein translocation between specific sites on different DNA molecules. J Am Chem Soc 129:13232–13237

Schuldiner S (2009) EmrE, a model for studying evolution and mechanism of ion-coupled transporters. Biochim Biophys Acta 1794:748 –762

Sekhar A et al (2015) Thermal fluctuations of immature SOD1 lead to separate folding and misfolding pathways. Elife 4:e07296

Tang C, Louis JM, Aniana A, Suh JY, Clore GM (2008) Visualizing transient events in amino-terminal autoprocessing of HIV-1 protease. Nature 455:693-U92

Tate CG, Ubarretxena-Belandia I, Baldwin JM (2003) Conformational changes in the multidrug transporter EmrE associated with substrate binding. J Mol Biol 332:229–242

Traaseth NJ et al (2012) Heteronuclear Adiabatic Relaxation Dispersion (HARD) for quantitative analysis of conformational dynamics in proteins. J Magn Reson 219:75–82

Tugarinov V, Kay LE (2005) Methyl groups as probes of structure and dynamics in NMR studies of high-molecular-weight proteins. Chembiochem 6:1567–1577

Ubarretxena-Belandia I, Baldwin JM, Schuldiner S, Tate CG (2003) Three-dimensional structure of the bacterial multidrug transporter EmrE shows it is an asymmetric homodimer. EMBO J 22:6175–6181

Ulrich EL et al (2008) BioMagResBank. Nucleic Acids Res 36:D402-8

Vallurupalli P, Bouvignies G, Kay LE (2012) Studying "invisible" excited protein states in slow exchange with a major state conformation. J Am Chem Soc 134:8148–8161

Ward KM, Aletras AH, Balaban RS (2000) A new class of contrast agents for MRI based on proton chemical exchange dependent saturation transfer (CEST). J Magn Reson 143:79–87

Xu X, Lee JS, Jerschow A (2013) Ultrafast scanning of exchangeable sites by NMR spectroscopy. Angew Chem Int Ed Engl 52:8281–8284

Zhao B, Guffy SL, Williams B, Zhang Q (2017) An excited state underlies gene regulation of a transcriptional riboswitch. Nat Chem Biol 13:968–974

Zhou JY, van Zijl PCM (2006) PChemical exchange saturation transfer imaging and spectroscopy. Prog Nucl Magn Reson Spectrosc 48:109–136